Spontaneous Ferromagnetism Induced Topological Transition in EuB_6

W. L. Liu,[1,2,3,*,‖] X. Zhang,[2,*] S. M. Nie,[4,*] Z. T. Liu,[1,*] X. Y. Sun,[2] H. Y. Wang,[2] J. Y. Ding,[1,3] Q. Jiang,[1,3] L. Sun,[5] F. H. Xue,[5] Z. Huang,[1] H. Su,[2] Y. C. Yang,[1] Z. C. Jiang,[1] X. L. Lu,[1,3] J. Yuan,[2] Soohyun Cho,[1] J. S. Liu,[1,3] Z. H. Liu,[1,3] M. Ye,[1,3] S. L. Zhang,[2] H. M. Weng,[6,7] Z. Liu,[2] Y. F. Guo,[2,†] Z. J. Wang,[6,7,‡] and D. W. Shen[1,3,§]

[1]*Center for Excellence in Superconducting Electronics, State Key Laboratory of Functional Materials for Informatics, Shanghai Institute of Microsystem and Information Technology, Chinese Academy of Sciences, Shanghai 200050, China*

[2]*School of Physical Science and Technology, ShanghaiTech University, Shanghai 201210, China*

[3]*Center of Materials Science and Optoelectronics Engineering, University of Chinese Academy of Sciences, Beijing 100049, China*

[4]*Department of Materials Science and Engineering, Stanford University, Stanford, California 94305, USA*

[5]*School of Information Science and Technology, ShanghaiTech University, Shanghai 201210, China*

[6]*Institute of Physics and Beijing National Laboratory for Condensed Matter Physics, Chinese Academy of Sciences, Beijing 100190, China*

[7]*University of Chinese Academy of Sciences, Beijing 100049, China*

(Received 8 March 2021; revised 9 August 2022; accepted 12 September 2022; published 13 October 2022)

The interplay between various symmetries and electronic bands topology is one of the core issues for topological quantum materials. Spontaneous magnetism, which leads to the breaking of time-reversal symmetry, has been proven to be a powerful approach to trigger various exotic topological phases. In this Letter, utilizing the combination of angle-resolved photoemission spectroscopy, magneto-optical Kerr effect microscopy, and first-principles calculations, we present the direct evidence on the realization of the long-sought spontaneous ferromagnetism induced topological transition in soft ferromagnetic EuB_6. Explicitly, we reveal the topological transition is from $Z_2 = 1$ topological insulator in paramagnetic state to $\chi = 1$ magnetic topological semimetal in low temperature ferromagnetic state. Our results demonstrate that the simple band structure near the Fermi level and rich topological phases make EuB_6 an ideal platform to study the topological phase physics.

DOI: 10.1103/PhysRevLett.129.166402

In the past decades, the investigation of topological phases has aroused a great deal of interest due to the breakthrough on the paradigm of condensed matter physics and various potential applications. One core issue of these research activities is to understand the interplay between all kinds of symmetries and topology [1]. In fact, topologically nontrivial materials are defined as a specific class of materials in which electronic structure can be classified by topological invariants protected by various symmetries [2–5]. Among them, time-reversal symmetry (TRS) is an important one and has attracted much attention. For example, it is TRS that protects the novel gapless helical surface states in topological insulator (TI) [6–9]. While, the breaking of TRS can significantly alter the electronic structure and may give rise to some exotic topological phases, such as the formation of magnetic Weyl nodes from topological trivial bands through the application of external magnetic field in half-Heusler compounds [10–12], and the realization of quantum anomalous Hall state through magnetic doping in TIs [13–16]. In particular, the search for topological transitions due to spontaneous time-reversal symmetry breaking (TRSB) is of particular interest for the interaction between intrinsic magnetism and topology may introduce a variety of novel physics [17–23]. For example, in two-dimensional (2D) ferromagnetic (FM) or antiferromagnetic TIs, spontaneous TRSB can lead to topological transitions to quantum anomalous Hall insulators [24–28] or topological axion insulators [29–34]. As for three-dimensional (3D) systems, spontaneous TRSB is as well expected to give rise to Weyl semimetals (WSM) or Wely nodal-line semimetals (WNLSM) [35–39]. Nevertheless, topological transitions directly driven by spontaneous magnetism have not been reported experimentally so far.

Recently, it was suggested that europium hexaboride (EuB_6), a typical soft magnetic material, should undergo a topological transition from a small gap semiconductor in its paramagnetic (PM) state to a TRS broken topological semimetal in the ferromagnetic state, considering that the effective magnetic exchange splitting renders opposite effect on the two bands and consequently leads to the band inversion in the spin-up subbands [39–42]. Previous angle-resolved photoemission spectroscopy (ARPES) studies on EuB_6 suggested an X-point band gap as large as 1 eV with the Fermi energy (E_F) near the bottom of the conduction band [43,44] and no sign of the band inversion, in conflict with the semimetal character with a small X-point band overlap revealed by bulk-sensitive techniques, such as the quantum oscillation [45,46].

Furthermore, a spin split surface state has been reported in a recent STM work [47]. EuB_6 becomes ferromagnetic below $T_{c2} = 12.5$ K, and the large negative magnetoresistance, which is related to percolation-type transition resulting from the overlap of magnetic polarons, occurs at another magnetic phase transition temperature $T_{c1} = 15.3$ K [48–54]. The experimental exploration of the low-lying electronic structure of EuB_6, particularly for the detailed evolution upon magnetic phase transition, would shed light on the comprehensive understanding of its nontrivial topological property.

In this Letter, combining ARPES, magneto-optical Kerr effect (MOKE) microscopy, and first-principles calculations, we have systematically investigated the evolution of bulk band structure with temperature in a soft magnetic material EuB_6 and provided a direct evidence for the realization of topological transition induced by the spontaneous ferromagnetism.

Details of our experiments and calculations can be found in the Supplemental Material (SM) [55]. EuB_6 has a CsCl-type structure with space group $Pm3m$ (no. 221) as shown in Fig. 1(a) [61]. Cleaving between Eu and B_6 octahedron planes will give two polar terminations, which have been confirmed by STM experiments [47]. The bulk and (001)-projected surface Brillouin zones (BZs) of EuB_6 are shown in Fig. 1(b). Our samples have been characterized by the single-crystal XRD (Fig. S1 of SM [55]), and the results along high-symmetry directions show individual dots with no impurity phases appearing, suggesting the excellent quality of these samples. After cleaving, the sample shows typical flat and shining surface. Moreover, the low-energy electron diffraction pattern, as shown in Fig. S1 (b) of SM [55] (*i*), confirms the square (001) cleavage surface of EuB_6.

In the first-principles calculations for paramagnetic EuB_6 (see Figs. S2 and S3 of SM [55]), the band overlap (gap) at X (Z) is sensitive to the internal parameter u, a parameter characterizing the relative size of the B_6 octahedron in one unit cell. Here, according to the XRD refinement on the very EuB_6 sample which we conducted ARPES measurements on, the lattice constant was determined to be 4.1851 Å, and the distances between two B atoms inside the octahedron and between two octahedrons are 1.7756 and 1.6740 Å, respectively, which suggest the internal parameter $u \sim 0.200$. Based on these crystal parameters, our calculation reveals a small band inversion between conduction and valence bands at three $X(Y, Z)$ points without spin-obit coupling (SOC) [Figs. 1(c) and 1(d)]. In fact, due to the absence of special symmetry protection, EuB_6 is a typical topological insulator after considering SOC. We note that this result is different from the conventional insulator with a small gap predicted for paramagnetic EuB_6 by the previous Letter [39], which is related to the sensitivity of band gap to the internal parameter u [62].

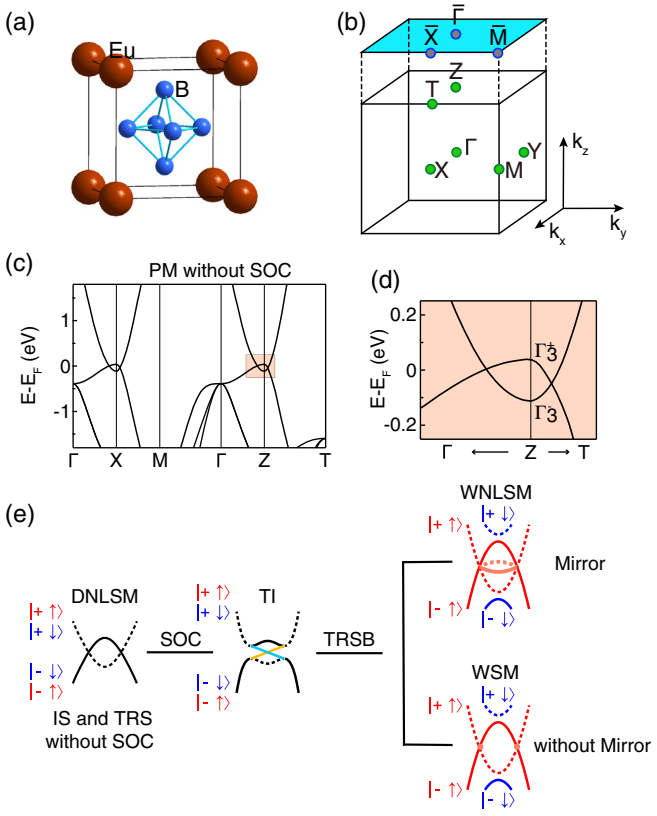

FIG. 1. (a) Crystal structure and (b) bulk and (001)-projected surface BZs of EuB_6. (c) Calculated band structure of EuB_6 in its paramagnetic state without SOC. The valence band and conduction band with opposite parity near E_F are labeled as Γ_3^- and Γ_3^+, respectively. Here the lattice constant $a = 4.1851$ Å and $u = 0.200$ are used, determined directly from the fitting of XRD data. (d) Enlargement of the band crossing at $Z(X, Y)$ point. (e) Schematic plot of emergent topological phases with TRSB in centrosymmetric 3D systems. "+" and "−" represent even and odd parity of corresponding band, and "↑" and "↓" represent spin-up and spin-down, respectively. Black bands are spin degenerated bulk bands, while red and blue bands are spin-up and spin-down branches, respectively. DNLSM (Dirac nodal line semimetal): without considering SOC, the spin degenerated conduction and valence band crossing with each other gives rise to the fourfold degenerate nodal line.

In the FM state, the exchange field will induce the spin splitting of the bulk bands. Interestingly, the relatively large exchange splitting would remove the original band inversion in the spin-down channel. However, the band inversion still exists and even becomes more prominent in the spin-up channel. Such a band inversion in this magnetic centrosymmetric system gives rise to the topological invariant $\chi = 1$; here, χ is defined by

$$(-1)^{\chi} \equiv \prod_{j=\{1,2,\ldots,n_{\mathrm{occ}}\},\Gamma_i=\mathrm{TRIMs}} \xi_i^j, \qquad (1)$$

where ξ_i^j is the parity eigenvalue of the jth band at the time-reversal-invariant-momentum (TRIM) Γ_i and n_{occ} is the

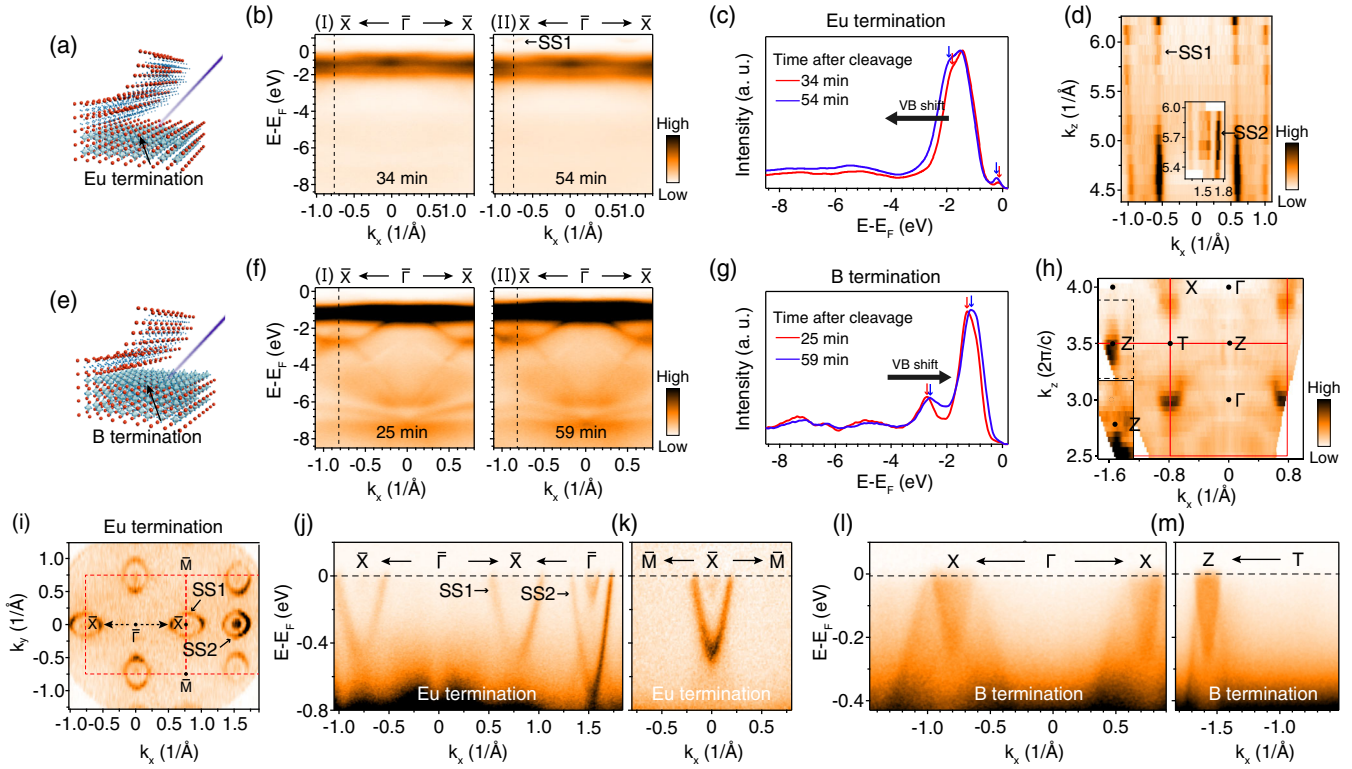

FIG. 2. (a) Sketch plot of the Eu termination surface. (b)(I),(II) Photoemission intensity plots along $\bar{\Gamma}-\bar{X}$ at different time after sample cleaved on the Eu termination surface. The probing photons are of 71 eV. (c) Energy distribution curve (EDCs) along the corresponding dashed lines in (b). (d) Photoemission intensity map on the k_x–k_z plane taken at E_F. Inset is the corresponding intensity map for the band SS2 [for details, see (i) and (j)]. (e) Sketch plot of the B termination surface. (f) (I),(II) ARPES intensity plots along $\bar{\Gamma}$–$\bar{X}$ at different time after sample cleaved on the B termination. Photons are of 71 eV. (g) EDCs along the corresponding dashed lines in (f). (h) Photoemission intensity map on the k_x–k_z plane taken at E_F with the photon-energy range from 40 to 136 eV. The inner potential of 15 eV was determined to match the periodicity along k_z. Inset is the intensity map taken at $E_F-0.2$ eV for the dashed square containing the Z point, suggesting the 3D character of the valence band. (i) Photoemission intensity map on the k_x–k_y plane of the Eu termination surface with an energy window of 50 meV. $\bar{\Gamma}$, $\bar{X}$, and $\bar{M}$ represent high-symmetry points in the projected two-dimensional BZ. (j),(k) Photoemission intensity plots of the Eu termination surface along $\bar{\Gamma}$–$\bar{X}$ and $\bar{M}$–$\bar{X}$, respectively. (l) Intensity plots on the B termination surface along the Γ–X direction with the photon energy 130 eV at 4.9 K. (m) Intensity plots on the B termination surface along the T–Z direction at 4.9 K with the photon energy 103 eV.

total number of the occupied bands. $\chi = 1$ guarantees that the band crossings cannot be fully gapped by SOC, making EuB_6 to be a magnetic topological semimetal [39]. Generally, it can be either a magnetic WSM or WNLSM, depending on whether the mirror symmetry is broken or not in the unit cell after considering the ordered magnetic moments as illustrated in Fig. 1(e).

By taking a comprehensive survey on the electronic structure of EuB_6 through synchrotron radiation-based mirco-ARPES (with a tiny 30×30 μm beam spot) and numerous attempts of cleavage, we achieved two sets of data with obvious contrasts between them. Previous ARPES studies on EuB_6 have revealed the gradually enlarger electron pocket with time [44]. A similar temporal change was also detected on one set of data, as shown in Figs. 2(b) and 2(c). More details about the temporal change on photoemission spectra can be found in Fig. S4 of SM [55]. Additionally, we found that the chemical potential of samples could be recovered when heated (Fig. S5 of SM [55]), demonstrating typical atomic adsorption effects on polar surfaces. The surface-state character of the bands SS1 in Fig. 2(b)(II) and SS2 in Fig. 2(j) is revealed by the negligible k_z dispersion in Fig. 2(d). On the contrary, on another set of data showing the opposite chemical potential shift with time [Figs. 2(f) and 2(g)], we found a clear dispersion with periodic modulation along k_z as shown in Fig. 2(h), which confirms their bulk-band nature. Moreover, in Fig. 2(b), only the electron pocket from Eu $5d$ orbitals and Eu $4f$ peak can be seen, while in contrast, the valence bands have strong intensity in Fig. 2(f). According to previous calculation of divalent hexaborides, the conduction band comes mainly from cation, while the low-energy valence band mainly consists of B-atom orbitals [62]. Thus we believe the distinct difference in the photoemission spectra between Figs. 2(b) and 2(f) is due to the surface sensitivity of ARPES. Based on this, we suggest

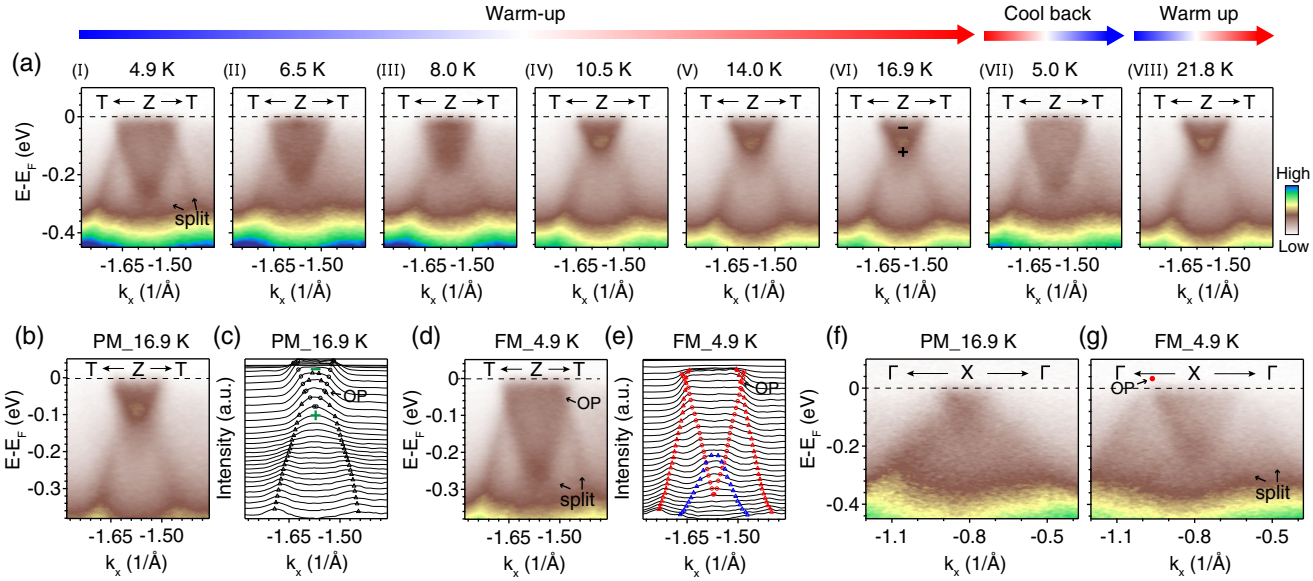

FIG. 3. (a) Photoemission intensity plots at different temperatures along the T–Z direction, which are also following the chronological order. Symbols "+" and "−" in (VI) indicate even and odd parity of occupied bands at Z, respectively. The probing photons are of 103 eV. (b),(c) Photoemission intensity plot and corresponding momentum distribution curves taken in the PM state along T–Z. OP represents the band overlap region. (d),(e) The same as (b) and (c), but taken in the FM state. (f),(g) Photoemission intensity plots taken along $\Gamma - X$ in the PM and FM states. The probing photons are of 130 eV.

that the data in Fig. 2(b) are mainly collected on Eu termination surface while in Fig. 2(f) it is collected on the B termination surface, which is further confirmed by detailed photoemission spectroscopic study on B 1s core level and Eu 4f spectra (Fig. S6 of SM [55]). The opposite shift direction of the chemical potential on these two termination surfaces shown in Figs. 2(c) and 2(g) might be caused by the opposite polarities of them. In addition, our calculation on a nine-layer slab indicates that the electron pockets SS1 and SS2 are mainly contributed by the outermost Eu atoms (Fig. S7 of SM [55]), consistent with our conclusion.

In Fig. 2(i), we present the intensity map at E_F on Eu termination surface in the FM state (9.5 K) after the adsorption saturation, in which two concentric circular electron pockets and two elliptical ones appear around the BZ center and boundary, respectively. The circular pockets are more clearly visible in the second BZ, and we note that this strong matrix element effect can also manifest itself on the bulk bands. The band dispersion along the high-symmetry directions on the Eu and B termination surface is shown in Figs. 2(i), 2(j), 2(l), and 2(m) for comparison.

Figure 3(a) illustrates the detailed evolution of bulk bands around the Z point with temperature. At the lowest temperature (4.9 K), the valence band is split into two branches due to the exchange coupling, and we then mark that crossing the Fermi level as the up branch (spin-up branch according to calculations) and the lower one crossing the bottom of the conduction band as the down branch [Fig. 3(e)]. As the temperature increases, the up branch keeps shifting downward while the down branch moves up, gradually shrinking the exchange splitting. Meanwhile, the down branch of the conduction band also hikes up with the rising temperature. Above 10.5 K, the splitting of the valence band can hardly be observed. After the measurement taken at 16.9 K, we then chilled the sample to ∼5 K to check whether the spectral change upon temperature is intrinsic or not. After confirming that our findings were well reproducible in the FM phase, we increased the temperature again to 21.8 K, well above the phase transition temperature. The nearly same spectra between Figs. 3(a)(VI) and 3(a)(VIII) further verified the temperature reversibility of the electronic structure changes crossing the phase transition. Moreover, we note that our MOKE data illustrate that magnetic domains start to form at nearly the same critical temperature [Fig. S8(a) in the SM [55]], indicating that the band splitting is indeed induced by the exchange field.

To directly compare the electronic structure in the PM and FM states, we present photoemission intensity plots and corresponding momentum distribution curves in Figs. 3(b)–3(e). In the PM state, the conduction and valence bands have an overlap in energy, which can be further confirmed by some other EuB_6 samples with less carrier density, as shown in Fig. S9 of SM [55]. Our calculations determined that the conduction and valence bands of EuB_6 should belong to the same irreducible representations when considering the SOC [see Fig. S10(b) of SM], and full gaps would definitely open at band crossings [55,63]. Because the inverted conduction and valence bands have opposite parities at three X (Y, Z) points, in the presence of both

inversion and time-reversal symmetries, we can unambiguously determine that paramagnetic EuB_6 is a topological insulator with $Z_2 = 1$ [64]. However, we note that the tiny SOC gap is hard to observe on the photoemission data, which might be due to its rather small energy size and the relatively low energy resolution (see more details in SM [55]). In the FM state, the exchange field results in the spin-up conduction band branch sinking and the spin-up valence band branch rising simultaneously. In this way, the band crossing in the spin-up channel would persist and becomes more prominent with the decrease of temperature. But as highlighted in Figs. 3(d) and 3(e), the spin-down conduction band branch has been pushed above E_F while the spin-down valence band branch shifts down to high binding energy, removing the original band inversion in spin-down channel.

As shown in Fig. 3(f), the band inversion can be further confirmed along the Γ–X direction in the PM state, while in the FM state the exchange splitting manifests itself as in Fig. 3(g). Unlike the band structure along T–Z, where the band overlap region is slightly below E_F, along this direction, the OP of the spin-up channel is slightly above the Fermi level, consisted with calculations [39]. This kind of band inversion at three X (Y, Z) points would give rise to $\chi = 1$, making EuB_6 to be a magnetic topological semimetal. Recently, one similar phase transition between different topological nontrivial states has been reported in $EuAs_3$ through transport measurements [65]. We note that our current findings are not fully consistent with the previous Letter [39] since the band inversion has been found to occur in the PM state. Such band evolution caused by the FM order is more systematically illustrated in Fig. 1(e).

In summary, we have successfully disentangled the three-dimensional bulk-band structure of EuB_6 on photoemission spectra. In the PM state, we have found the band inversion at three X (Y, Z) points of EuB_6, and it can be assigned as a topological insulator with $Z_2 = 1$. When EuB_6 undergoes the FM transition confirmed by our MOKE experiments, the bulk states split, and we have found that the band inversion only remains in one spin channel due to the relatively large exchange splitting at low temperatures. Thus, it would make EuB_6 to be a magnetic topological semimetal with $\chi = 1$. Our Letter provides a direct evidence on the topological transition in EuB_6 induced by the spontaneous ferromagnetism.

This work was supported by the National Science Foundation of China (Grants No. U2032208, No. 11874264, and No. 12222413), the National Key R&D Program of the MOST of China (Grant No. 2016YFA0300204), and the Natural Science Foundation of Shanghai (Grants No. 14ZR1447600 and No. 22ZR1473300). Y. F. G. acknowledges the starting grant of ShanghaiTech University and the Program for Professor of Special Appointment (Shanghai Eastern Scholar). Z. J. W. was supported by the National Nature Science Foundation of China (Grants No. 11974395 and No. 12188101), the Strategic Priority Research Program of Chinese Academy of Sciences (Grant No. XDB33000000), and the Center for Materials Genome. J. S. L. thanks the fund of Science and Technology on Surface Physics and Chemistry Laboratory (6142A02200102). Part of this research used beam line 03U of the Shanghai Synchrotron Radiation Facility, which is supported by the ME^2 project under Contract No. 11227902 from National Natural Science Foundation of China. The authors also thank Analytical Instrumentation Center (No. SPST-AIC10112914), SPST, ShanghaiTech University, for support.

Note added.—Recently, a photoemission work, which reports some results that are similar to part of our findings and was carried out independently by another group, was published [66].

*These authors contributed equally to this work.
†guoyf@shanghaitech.edu.cn
‡wzj@iphy.ac.cn
§dwshen@mail.sim.ac.cn
‖Present address: Institute of Advanced Science Facilities, Shenzhen, Guangdong, 518107, China.

[1] C.-K. Chiu, J. C. Y. Teo, A. P. Schnyder, and S. Ryu, Rev. Mod. Phys. **88**, 035005 (2016).
[2] N. P. Armitage, E. J. Mele, and A. Vishwanath, Rev. Mod. Phys. **90**, 015001 (2018).
[3] M. Z. Hasan and C. L. Kane, Rev. Mod. Phys. **82**, 3045 (2010).
[4] B.-H. Yan and C. Felser, Annu. Rev. Condens. Matter Phys. **8**, 337 (2017).
[5] S.-Y. Yang, H. Yang, E. Derunova, S. S. P. Parkin, B.-H. Yan, and M. N. Ali, Adv. Phys. X **3**, 1414631 (2018).
[6] X.-L. Qi and S.-C. Zhang, Rev. Mod. Phys. **83**, 1057 (2011).
[7] Y.-L. Chen, J. G. Analytis, J.-H. Chu, Z.-K. Liu, S.-K. Mo, X.-L. Qi, H.-J. Zhang, D.-H. Lu, X. Dai, and Z. Fang, Science **325**, 178 (2009).
[8] D. Hsieh, Y. Xia, D. Qian, L. Wray, J. H. Dil, F. Meier, J. Osterwalder, L. Patthey, J. G. Checkelsky, N. P. Ong, A. V. Fedorov, H. Lin, A. Bansil, D. Grauer, Y. S. Hor, R. J. Cava, and M. Z. Hasan, Nature (London) **460**, 1101 (2009).
[9] H.-J. Zhang, C.-X. Liu, X.-L. Qi, X. Dai, Z. Fang, and S.-C. Zhang, Nat. Phys. **5**, 438 (2009).
[10] K. Manna, Y. Sun, L. Muechler, J. Kübler, and C. Felser, Nat. Rev. Mater. **3**, 244 (2018).
[11] S. Chadov, X. Qi, J. Kubler, G. H. Fecher, C. Felser, and S.-C. Zhang, Nat. Mater. **9**, 541 (2010).
[12] H. Lin, L. A. Wray, Y. Xia, S. Xu, S. Jia, R. J. Cava, A. Bansil, and M. Z. Hasan, Nat. Mater. **9**, 546 (2010).
[13] R. Yu, W. Zhang, H.-J. Zhang, S.-C. Zhang, X. Dai, and Z. Fang, Science **329**, 61 (2010).
[14] C.-Z. Chang *et al.*, Science **340**, 167 (2013).
[15] X. Kou, S.-T. Guo, Y. Fan, L. Pan, M. Lang, Y. Jiang, Q. Shao, T. Nie, K. Murata, J. Tang, Y. Wang, L. He, T.-K. Lee,

W.-L. Lee, and K. L. Wang, Phys. Rev. Lett. **113**, 137201 (2014).
[16] J. Wang, B. Lian, and S.-C. Zhang, Phys. Scr. T **164**, 014003 (2015).
[17] B. Chen *et al.*, Nat. Commun. **10**, 4469 (2019).
[18] C.-W. Hu, L. Ding, K. N. Gordon, B. Ghosh, and N. Ni, Sci. Adv. **6**, eaba4275 (2020).
[19] J.-H. Li, C. Wang, Z.-T. Zhang, B.-L. Gu, W.-H. Duan, and Y. Xu, Phys. Rev. B **100**, 121103(R) (2019).
[20] M. M. Otrokov, I. P. Rusinov, M. Blanco-Rey, M. Hoffmann, A. Y. Vyazovskaya, S. V. Eremeev, A. Ernst, P. M. Echenique, A. Arnau, and E. V. Chulkov, Phys. Rev. Lett. **122**, 107202 (2019).
[21] S. Huan, S. Zhang, Z. Jiang, H. Su, H. Wang, X. Zhang, Y. Yang, Z. Liu, X. Wang, N. Yu, Z. Zou, D. Shen, J. Liu, and Y. Guo, Phys. Rev. Lett. **126**, 246601 (2021).
[22] S. Nie, G. Xu, F. B. Prinz, and S.-c. Zhang, Proc. Natl. Acad. Sci. U.S.A. **114**, 10596 (2017).
[23] G. Hua, S. Nie, Z. Song, R. Yu, G. Xu, and K. Yao, Phys. Rev. B **98**, 201116(R) (2018).
[24] R. Yu, W. Zhang, H.-J. Zhang, S.-C. Zhang, X. Dai, and Z. Fang, Science **329**, 61 (2010).
[25] C.-Z. Chang, J.-S. Zhang, X. Feng, J. Shen, and Q.-K. Xue, Science **340**, 167 (2013).
[26] H.-J. Zhang, Y. Xu, J. Wang, K. Chang, and S.-C. Zhang, Phys. Rev. Lett. **112**, 216803 (2014).
[27] C.-Z. Chang, W. Zhao, D.-Y. Kim, H. Zhang, B. A. Assaf, D. Heiman, S.-C. Zhang, C. Liu, M.-H. Chan, and J. S. Moodera, Nat. Mater. **14**, 473 (2015).
[28] S. Nie, H. Weng, and F. B. Prinz, Phys. Rev. B **99**, 035125 (2019).
[29] D. M. Nenno, C. A. C. Garcia, J. Gooth, C. Felser, and P. Narang, Nat. Rev. Phys. **2**, 682 (2020).
[30] D. Zhang, M. Shi, T. Zhu, D. Xing, H. Zhang, and J. Wang, Phys. Rev. Lett. **122**, 206401 (2019).
[31] D. Xiao, J. Jiang, J. H. Shin, W. Wang, F. Wang, Y.-F. Zhao, C. Liu, W. Wu, M. H. W. Chan, N. Samarth, and C.-Z. Chang, Phys. Rev. Lett. **120**, 056801 (2018).
[32] C. Liu, Y. Wang, H. Li, Y. Wu, Y. Li, J. Li, K. He, Y. Xu, J. Zhang, and Y. Wang, Nat. Mater. **19**, 522 (2020).
[33] M. Mogi, M. Kawamura, R. Yoshimi, A. Tsukazaki, Y. Kozuka, N. Shirakawa, K. S. Takahashi, M. Kawasaki, and Y. Tokura, Nat. Mater. **16**, 516 (2017).
[34] Y. Hou and R. Wu, Nano Lett. **19**, 2472 (2019).
[35] D. F. Liu, A. J. Liang, E. K. Liu, Q. N. Xu, Y. W. Li, C. Chen, D. Pei, W. J. Shi, S. K. Mo, P. Dudin, T. Kim, C. Cacho, G. Li, Y. Sun, L. X. Yang, Z. K. Liu, S. S. P. Parkin, C. Felser, and Y. L. Chen, Science **365**, 1282 (2019).
[36] N. Morali, R. Batabyal, P. K. Nag, E. Liu, Q. Xu, Y. Sun, B. Yan, C. Felser, N. Avraham, and H. Beidenkopf, Science **365**, 1286 (2019).
[37] E. Liu *et al.*, Nat. Phys. **14**, 1125 (2018).
[38] Q. Wang, Y. Xu, R. Lou, Z. Liu, M. Li, Y. Huang, D. Shen, H. Weng, S. Wang, and H. Lei, Nat. Commun. **9**, 3681 (2018).
[39] S. Nie, Y. Sun, F. B. Prinz, Z. Wang, H. Weng, Z. Fang, and X. Dai, Phys. Rev. Lett. **124**, 076403 (2020).
[40] J. Kuneš and W. E. Pickett, Phys. Rev. B **69**, 165111 (2004).
[41] J. Kim, W. Ku, C.-C. Lee, D. S. Ellis, B. K. Cho, A. H. Said, Y. Shvyd'ko, and Y.-J. Kim, Phys. Rev. B **87**, 155104 (2013).
[42] D. Sheets, V. Flynn, J. Kim, M. Upton, D. Casa, T. Gog, Z. Fisk, M. Dzero, P. F. S. Rosa, D. G. Mazzone, I. Jarrige, J.-X. Zhu, and J. Hancock, J. Phys. Condens. Matter **32**, 135601 (2020).
[43] J. D. Denlinger, J. A. Clack, J. W. Allen, G. H. Gweon, D. M. Poirier, C. G. Olson, J. L. Sarrao, A. D. Bianchi, and Z. Fisk, Phys. Rev. Lett. **89**, 157601 (2002).
[44] J. D. Denlinger, G. H. Gweon, S.-K. Mo, J. W. Allen, J. L. Sarrao, A. D. Bianchi, and Z. Fisk, J. Phys. Soc. Jpn. **71**, 1 (2002).
[45] R. G. Goodrich, N. Harrison, J. J. Vuillemin, A. Teklu, D. W. Hall, Z. Fisk, D. Young, and J. Sarrao, Phys. Rev. B **58**, 14896 (1998).
[46] M. C. Aronson, J. L. Sarrao, Z. Fisk, M. Whitton, and B. L. Brandt, Phys. Rev. B **59**, 4720 (1999).
[47] S. Rößler, L. Jiao, S. Seiro, P. F. S. Rosa, Z. Fisk, U. K. Rößler, and S. Wirth, Phys. Rev. B **101**, 235421 (2020).
[48] S. Süllow, I. Prasad, M. C. Aronson, J. L. Sarrao, Z. Fisk, D. Hristova, A. H. Lacerda, M. F. Hundley, A. Vigliante, and D. Gibbs, Phys. Rev. B **57**, 5860 (1998).
[49] P. Das, A. Amyan, J. Brandenburg, J. Müller, P. Xiong, S. von Molnár, and Z. Fisk, Phys. Rev. B **86**, 184425 (2012).
[50] R. R. Urbano, P. G. Pagliuso, C. Rettori, S. B. Oseroff, J. L. Sarrao, P. Schlottmann, and Z. Fisk, Phys. Rev. B **70**, 140401(R) (2004).
[51] S. Süllow, I. Prasad, M. C. Aronson, S. Bogdanovich, J. L. Sarrao, and Z. Fisk, Phys. Rev. B **62**, 11626 (2000).
[52] X. Zhang, L. Yu, S. von Molnár, Z. Fisk, and P. Xiong, Phys. Rev. Lett. **103**, 106602 (2009).
[53] M. L. Brooks, T. Lancaster, S. J. Blundell, W. Hayes, F. L. Pratt, and Z. Fisk, Phys. Rev. B **70**, 020401(R) (2004).
[54] T. Fujita, M. Suzuki, and Y. Ishikawa, Solid State Commun. **33**, 947 (1980).
[55] See Supplemental Material at http://link.aps.org/supplemental/10.1103/PhysRevLett.129.166402 for details of methods (single-crystal synthesis and characterization, MOKE, ARPES, and calculations), which includes Refs. [56–60].
[56] Y.-C. Yang, Z.-T. Liu, J.-S. Liu, Z.-H. Liu, W.-L. Liu, X.-L. Lu, H.-P. Mei, A. Li, M. Ye, S. Qiao, and D.-W. Shen, Nucl. Sci. Tech. **32**, 1 (2021).
[57] G. Kresse and J. Furthmüller, Phys. Rev. B **54**, 11169 (1996).
[58] G. Kresse and J. Furthmüller, Comput. Mater. Sci. **6**, 15 (1996).
[59] J. P. Perdew, K. Burke, and M. Ernzerhof, Phys. Rev. Lett. **77**, 3865 (1996).
[60] A. I. Liechtenstein, V. I. Anisimov, and J. Zaanen, Phys. Rev. B **52**, R5467 (1995).
[61] Y. Takahashi, M. Fujimoto, M. Tsuchiko, and K. I. Ohshima, J. Appl. Crystallogr. **34**, 208 (2001).
[62] S. Massiddam, A. Continenza, T. de Pascale, and R. Monnier, Physica (Amsterdam) **102B**, 83 (1996).
[63] Q. D. Gibson, L. M. Schoop, L. Muechler, L. S. Xie, M. Hirschberger, N. P. Ong, R. Car, and R. J. Cava, Phys. Rev. B **91**, 205128 (2015).

[64] L. Fu and C. L. Kane, Phys. Rev. B **76**, 045302 (2007).
[65] E. Cheng, W. Xia, X. Shi, H. Fang, C. Wang, C. Xi, S. Xu, D. C. Peets, L. Wang, H. Su *et al.*, Nat. Commun. **12**, 1 (2021).
[66] S.-Y. Gao, S. Xu, H. Li, C.-J. Yi, S.-M. Nie, Z.-C. Rao, H. Wang, Q.-X. Hu, X.-Z. Chen, W.-H. Fan, J.-R. Huang, Y.-B. Huang, N. Pryds, M. Shi, Z.-J. Wang, Y.-G. Shi, T.-L. Xia, T. Qian, and H. Ding, Phys. Rev. X **11**, 021016 (2021).